ACS OMEGA

http://pubs.acs.org/journal/acsodf
Article

Synthesis and Characterization of NaX Zeolite from Coal Gangue and Its Efficacy in Cd and Pb Remediation in Water and Soil

Zhibing Chang, Yinuo Yan, Lu Bai,* Nan Guo, Zhenguo Xing, and Chunwei Lu

Cite This: *ACS Omega* 2024, 9, 51237−51252
Read Online

ACCESS | Metrics & More | Article Recommendations | Supporting Information

ABSTRACT: Alkaline fusion is a pivotal process influencing the cost of synthesizing zeolite from coal gangue. This study examined the effects of alkaline fusion temperature (X_1), treatment duration (X_2) and the NaOH/coal gangue weight ratio (X_3) on the composition and properties of the products, as well as their adsorption capacities for Cd^{2+} ($q_{e,Cd}$) and Pb^{2+} ($q_{e,Pb}$). Response surface methodology (RSM) was employed to analyze the interactions among these factors, and the adsorption mechanisms for Cd^{2+} and Pb^{2+} were investigated using X-ray diffraction, scanning electron microscopy-EDS, Fourier transform infrared, X-ray photoelectron spectroscopy, and N_2 adsorption−desorption techniques. The results reveal that (1) under optimized conditions−X_1 of approximately 800 °C, X_2 of around 2.8 h and X_3 of 1.2−the maximum $q_{e,Cd}$ and $q_{e,Pb}$ for the synthesized NaX zeolite can reach 181.3 and 419.9 mg/g, respectively. (2) The RSM models indicate that increasing the X_3 value can lower the required X_1. For $q_{e,Cd}$ and $q_{e,Pb}$ of 150 and 350 mg/g, respectively, with X_2 fixed at 2 h, increasing X_3 from 0.976 to 1.134 and from 0.900 to 1.289 enables a reduction in X_1 from 800 to 600 °C. (3) NaX zeolite primarily adsorbs Cd^{2+} and Pb^{2+} through ion exchange, allowing these ions to enter the zeolite's cage structure. Pb^{2+} can also precipitate as hydrocerussite ($Pb_3(CO_3)_2(OH)_2$) within the zeolite channels, while Cd^{2+} has a more significant impact on the [SiO_4] and [AlO_4] tetrahedra. (4) The synthesized NaX zeolite effectively reduces the exchangeable Cd content in contaminated soil from 3.51 to below 1.5 mg/kg. The remediation performance of the NaX zeolite for Cd and Pb in water and soil can be further enhanced by optimizing its Si/Al ratio and pore structure.

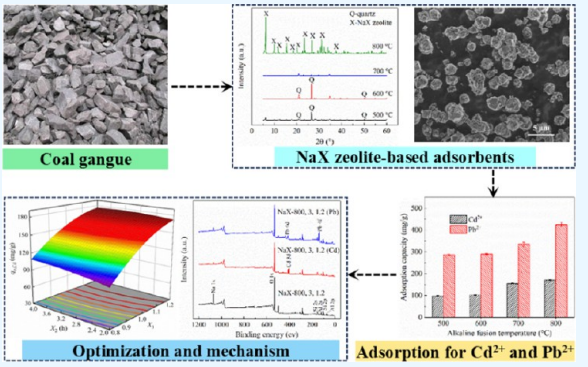

1. INTRODUCTION

As China's economy progresses, the concentration of heavy metal ions in solid waste generated during urbanization and industrialization processes is steadily rising. These ions can infiltrate soil and water, posing serious risks to both environments. According to the National Soil Pollution Status Survey Bulletin, the exceedance rates of Cd and Pb in Chinese soil samples are 7.0 and 1.5%, respectively, affecting approximately 20 million hectares of cultivated land.[1] Heavy metals accumulate in agricultural products and enter the human body through the food chain, posing significant health risks and leading to consecutive public health incidents related to heavy metal pollution in certain regions.[2] Therefore, urgent remediation efforts are necessary to address Cd and Pb pollution.

The primary methods for remediating heavy metal pollution include membrane separation, chemical precipitation, ultrafiltration, adsorption, ion exchange, electrolysis, evaporation, and biological approaches.[3] Among these, adsorption is particularly favored due to its simplicity, cost-effectiveness, high selectivity for target metals, and minimal introduction of new pollutants. Effective preparation of adsorbents is critical for successful implementation of this method.[4,5] Conversely, coal gangue, a substantial solid waste from coal mining and processing, typically contains high levels of SiO_2 and Al_2O_3 ranging from 60 to 90%. It serves as a natural raw material for synthesizing zeolite molecular sieves. The utilization of coal gangue in zeolite synthesis not only reduces the cost of zeolite production but also helps mitigate the environmental hazards associated with coal gangue, aligning with the principle of "using waste to process waste". This approach has garnered significant attention from researchers across various fields.

Alkaline fusion-assisted hydrothermal crystallization is the most common method used to synthesize zeolite. NaX zeolite, NaY zeolite and NaA zeolite were prepared and their adsorption behavior for heavy metal ions were explored.[7−10] For example, Lu et al.[7] synthesized zeolite NaX from coal gangue and reported that the removal of Co^{2+} and Cu^{2+} was controlled by surface adsorption, intraparticle diffusion, and film diffusion. They also found that the specific surface and

Received: August 20, 2024
Revised: December 2, 2024
Accepted: December 4, 2024
Published: December 16, 2024

Table 1. Main Chemical Composition of the Coal Gangue

SiO_2	Al_2O_3	Fe_2O_3	K_2O	Na_2O	CaO	MgO	SO_3	P_2O_5	others
64.64	21.43	3.56	3.59	0.87	2.51	0.92	0.3	0.18	2.00

pore volume of NaX zeolite increased with increasing SiO_2/Al_2O_3 ratio.[11] Physical adsorption and ion exchange were identified as the main removal mechanism of heavy metal ion.[9,12] Furthermore, the adsorption behavior transitioned from multimolecular layer adsorption to monomolecular layer adsorption as the ionic radius increased.[13] In order to improve adsorption performance, Bu et al.[14] developed a sequential alkaline and ultrasonic post-treatment method that facilitates the creation of hierarchical mesopores, thereby enhancing the adsorption performance of mesoporous zeolites. Li et al.[15,16] developed a composite material of zeolite and activated carbon utilizing coal gangue and coal as starting materials. The zeolite's uniform micropores enhance the adsorption capacity for heavy metal ions, whereas the hierarchical porous structure of the activated carbon is adept at capturing larger organic molecules.

The synthesized zeolite can also be used for the soil remediation, which can efficiently reduce the bioavailability and mobility of heavy metal ions in soil.[17,18] Zheng et al.[17] and Yang et al.[18] proposed the "soil for soil remediation" strategy and utilized soil resources to prepare the cancrinite (CAN) type of zeolite, which could suppress the uptake of Cd, As, Pb and Cu ions in the vegetables. To increase the immobilization performance of the zeolite passivator, some researchers used zeolite and other functionalized materials together.[19−21] For example, Gondek et al.[19] and Ibrahim et al.[20] used zeolite and biochar as the functionalized materials, they emphasized better results could be obtained by using these materials together for immobilizing heavy metals. Moreover, the adsorption properties of zeolite can also be improved by modification using inorganic salts, acids, organic molecules and supercritical water.[22−25] Ma et al.[24] prepared modified zeolite through a series of treatments including NaCl pretreatment, chitosan modification, chitosan loading and $CaSiO_3$ modification. Their findings indicated that these modifications significantly enhanced the cation exchange capacity and specific surface area of the zeolite, thereby stabilizing heavy metals in soil and reducing their leaching risk and bioavailability to organisms and plants.

The synthesis of zeolite via alkaline fusion-assisted hydrothermal crystallization involves multiple factors, with alkaline fusion temperature, fusion time and alkali dosing amount significantly affecting both energy consumption and processing costs. Although numerous studies have optimized conditions for synthesizing zeolite from coal gangue and have examined the adsorption capabilities of zeolite for heavy metal ions, there remains a lack of understanding regarding how these factors, particularly their interactions, influence adsorption performance. This knowledge gap is critical for advancing the industrial-scale production of zeolite from coal gangue. This paper investigated the effects of alkaline fusion temperature, processing duration and alkali amount on zeolite structure and its adsorption efficiency for Cd^{2+} and Pb^{2+}. Response surface methodology (RSM) was employed to systematically analyze the complex interactions among these factors, while X-ray diffraction (XRD), scanning electron microscopy (SEM)-energy dispersive X-ray spectroscopy (EDS), Fourier transform infrared (FTIR), and N_2 adsorption−desorption techniques were used to elucidate the adsorption mechanisms.

2. EXPERIMENTAL SECTION

2.1. Raw Materials. Coal gangue was collected from the Yangshita Mine in Erdos, Inner Mongolia. The chemical composition was analyzed using X-ray fluorescence spectroscopy (XRF-1800, Shimadzu), and the results are presented in Table 1. The molar ratio of SiO_2 to Al_2O_3 was found to be approximately 5.1. The raw coal gangue was crushed and screened to particles smaller than 180 μm, then dried at 105 °C for 24 h. The dried coal gangue was subsequently used for zeolite synthesis. Other chemicals such as $CdCl_2{\cdot}2.5H_2O$, $Pb(NO_3)_2$, NaOH and HCl were purchased from Sinopharm Chemical Reagent Co., Ltd.

2.2. Zeolite Synthesis. The alkaline fusion-assisted hydrothermal crystallization method used for zeolite synthesis involves the following steps: (1) Solid NaOH was added to coal gangue, and the mixture was calcined in a muffle furnace. (2) The resulting alkaline product was ground, mixed with deionized water at a ratio of 4 mL/g, and the slurry was stirred at 25 °C for 12 h. (3) The mixture was then moved to a stainless-steel reactor coated with polytetrafluoroethylene and heated to 100 °C for 8 h. (4) Afterward, the resulting product was collected through filtration, thoroughly washed with deionized water until the pH reached a stable level of 7, and dried at 105 °C for 2 h. To determine the ideal conditions for zeolite synthesis, a single-factor experimental design was conducted, with the specific parameters outlined in Table 2.

Table 2. Reaction Condition of Experiments

run no.	alkaline fusion temperature (°C)	alkaline fusion time (h)	NaOH/coal gangue ratio
	effect of alkaline fusion temperature		
1	500	3	1.0
2	600		
3	700		
4	800		
	effect of alkaline fusion time		
5	800	1	1.0
6		2	
7		3	
8		4	
	effect of NaOH dosing amount		
9	800	3	0.6
10			0.8
11			1.0
12			1.2

The reaction conditions explored include alkaline fusion temperatures ranging from 500 to 800 °C, alkaline fusion times of 1−4 h and NaOH/coal gangue weight ratios from 0.6 to 1.2.

2.3. Box-Behnken Method. RSM is a statistical approach that utilizes structured experimental designs to gather data and employs quadratic regression models to characterize the relationships between independent variables and response

https://doi.org/10.1021/acsomega.4c07708
ACS Omega 2024, 9, 51237−51252

outcomes. Through the analysis of these quadratic regression equations, RSM seeks to determine optimal process conditions and tackle issues involving multiple variables in optimization. The Box−Behnken method of RSM was employed to design experiments and establish a model using Design Expert software. Consequently, a series of experiments were conducted to optimize experimental parameters and predict the maximum adsorption capacity. The experimental parameters are presented in Table 3. The effective factors selected are

Table 3. Experimental Design in the Box-Behnken Method

run no.	X_1 (°C)	X_2 (h)	X_3	$q_{e,Cd}$ (mg/g)	$q_{e,Pb}$ (mg/g)
1	800	2	1	160.00	392.65
2	700	4	0.8	107.59	300.23
3	700	3	1	148.33	327.50
4	800	4	1	166.90	416.14
5	700	3	1	155.91	346.59
6	800	3	1.2	183.34	427.50
7	600	4	1	135.03	336.59
8	700	3	1	150.57	336.56
9	700	4	1.2	177.72	396.44
10	600	2	1	128.47	268.41
11	700	2	1.2	173.03	385.83
12	600	3	0.8	100.09	219.92
13	700	2	0.8	94.64	236.59
14	800	3	0.8	106.66	306.29
15	700	3	1	153.60	333.86
16	700	3	1	156.42	343.41
17	600	3	1.2	162.47	357.80

alkaline fusion temperature (X_1), alkaline fusion time (X_2) and NaOH/coal gangue weight ratio (X_3). The adsorption capacities of Cd^{2+} and Pb^{2+} were considered as the response variables. These parameters were varied within the upper and lower limits derived from single-factor experiments under specified experimental conditions. Since we identified the formation of NaX zeolite, the derived products were designated as NaX-X_1, X_2, X_3. For example, NaX-800, 3, 1.2 refers to the product from run 6 in Table 3.

2.4. Adsorption of Cd^{2+} and Pb^{2+} in Aqueous Solution. For the adsorption capacity experiment, solutions of Cd^{2+} and Pb^{2+} with a concentration of 100 mg/L were prepared by dissolving precise amounts of $CdCl_2{\cdot}2.5H_2O$ and $Pb(NO_3)_2$ in distilled water. The pH values of the Cd^{2+} and Pb^{2+} solutions were approximately 6 and 5, respectively. A volume of 50 mL of the Cd^{2+} solution or 100 mL of the Pb^{2+} solution was pipetted into a conical flask to simulate wastewater. Subsequently, 0.02 g of the solid product derived from coal gangue was added to the wastewater. The mixture was incubated at 25 °C for 180 min on a horizontal shaker. Following the adsorption period, the samples were filtered through a 0.45 μm membrane filter, and the concentrations of Cd^{2+} and Pb^{2+} were analyzed using a Mapada UV-1100 UV−visible spectrophotometer.[26] A briefly description of the test method can be seen in the Supporting Information. The adsorption capacity was determined according to Formula 1.

$$q_e = \frac{(c_0 - c_e) \times V}{m} \quad (1)$$

where q_e represents the adsorption capacity or the amount of metal ion adsorbed at equilibrium (mg/g), c_0 and c_e denote the initial and equilibrium concentrations of heavy metal ions, respectively (mg/L), V is the volume of the wastewater (L), and m is the mass of the solid product added to the flask (g). Additionally, $q_{e,Cd}$ and $q_{e,pb}$ refer to the adsorption capacities for Cd^{2+} and Pb^{2+}, respectively. The removal efficiency was calculated by using Formula 2.

$$R = \frac{(c_0 - c_e) \times 100}{c_0} \quad (2)$$

where R represents the removal efficiency (%). Each adsorption test was conducted in triplicate, and the average values were used as the final data. Moreover, adsorption tests were conducted at varying adsorption times, initial concentrations, pH levels and adsorbent dosages to investigate the influence of these parameters on the adsorption process. The detailed experimental procedure can be found in the Supporting Information.

2.5. Material Characterization. XRD, scanning electron microscope-energy dispersive spectroscopy (SEM-EDS), Fourier-transform infrared (FTIR), X-ray photoelectron spectroscopy (XPS), and N_2 adsorption−desorption isotherms were performed on the synthesized products. Detailed descriptions of these characterization methods are provided in the Supporting Information.

2.6. Stabilization of Cd in Soils. The contaminated soil sample was collected from the closed dumping site of the Buertai coal mine in Erdos, Inner Mongolia. The soil, contaminated by overlying coal gangue, has a notably high content of Cd. The sample was air-dried and sieved to remove particles larger than 20 mesh. The selected NaX zeolite samples were mixed with the contaminated soil at a weight percentage of 5%, while nonamended soil served as the control. The mixtures were combined with 25% distilled water and incubated in a cool, dark place for 3 weeks. Following incubation, the mixtures were dried at 60 °C for 24 h. All samples, including a control without zeolite, underwent Tessier sequential extraction according to the procedure outlined by Xiong et al.[27] Cd in the soil was fractionated into five categories: exchangeable, carbonate-bound, Fe−Mn oxides-bound, organic matter-bound and residual.

3. RESULTS AND DISCUSSION

3.1. Effect of Different Parameters on Zeolite Synthesis. *3.1.1. Effect of Alkaline Fusion Temperature on Zeolite Synthesis.* Figure 1 illustrates the effects of alkaline fusion temperature on the XRD pattern, SEM image and adsorption capacity of the synthesized product. Figure 1a shows that zeolite synthesis is minimal at alkaline fusion temperatures between 500 and 700 °C. Quartz persisted in the products resulting from alkaline fusion at both 500 and 600 °C. These results suggest that lower alkaline fusion temperatures are insufficient to activate the inherent minerals (e.g., kaolinite, Illite and quartz) in the coal gangue.[28] Zeolite NaX was successfully synthesized at an alkaline fusion temperature of 800 °C, indicating a higher activation efficiency at this temperature compared to the lower ones. The initial molar ratio of SiO_2/Al_2O_3 significantly affects the type of zeolite that is formed. Coal gangue with a lower SiO_2/Al_2O_3 ratio typically produces zeolite NaA, while a higher ratio promotes the formation of NaX and NaY.[29] In this study, zeolite NaX was synthesized from coal gangue with a high SiO_2/Al_2O_3 ratio of 5.1. Additionally, Chen et al.[11] were able to synthesize zeolite

https://doi.org/10.1021/acsomega.4c07708
ACS Omega 2024, 9, 51237−51252

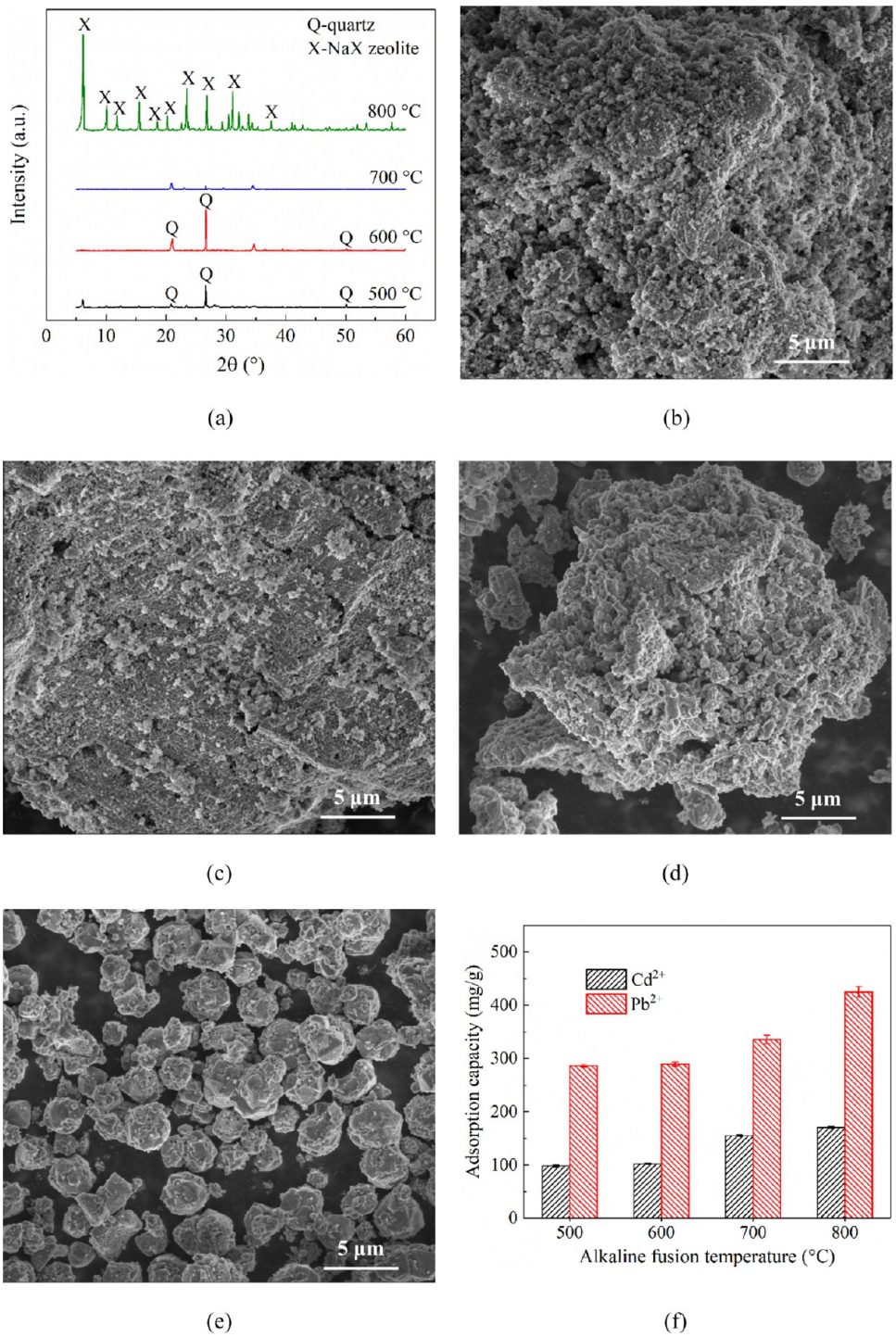

Figure 1. Impact of alkaline fusion temperature on the XRD pattern, SEM image and adsorption capacity of the synthesized product. (a) XRD patterns. (b–e) SEM images of the product derived from 500, 600, 700, and 800 °C fusion. (f) adsorption capacity.

NaX from coal gangue with a low SiO_2/Al_2O_3 ratio by adding a silicon source or using acid pretreatment.

Figure 1b–e indicate that the products formed at temperatures between 500 and 700 °C are predominantly amorphous. These products exhibit large particle sizes with fine particles adhering to their surfaces. Although not very prominent, small cubic particles were observed in the product obtained at 700 °C, which are believed to be zeolite or its precursor. At the higher fusion temperature of 800 °C, NaX zeolite particles with crystal sizes ranging from 2 to 5 μm were produced. The well-crystallized NaX zeolite exhibits an octahedral shape with a smooth surface.[11] The relatively low crystallinity observed may be attributed to suboptimal conditions during the aging and crystallization processes.

Figure 1f demonstrates that as the fusion temperature increases from 500 to 800 °C, the values of $q_{e,Cd}$ and $q_{e,Pb}$ rise progressively from 98.5 and 286.6 to 170.6 and 425.2 mg, respectively. This observed trend can be attributed to the characteristics of NaX zeolite, which include a high surface area, a stable crystal structure, a substantial cavity volume and a

https://doi.org/10.1021/acsomega.4c07708
ACS Omega 2024, 9, 51237−51252

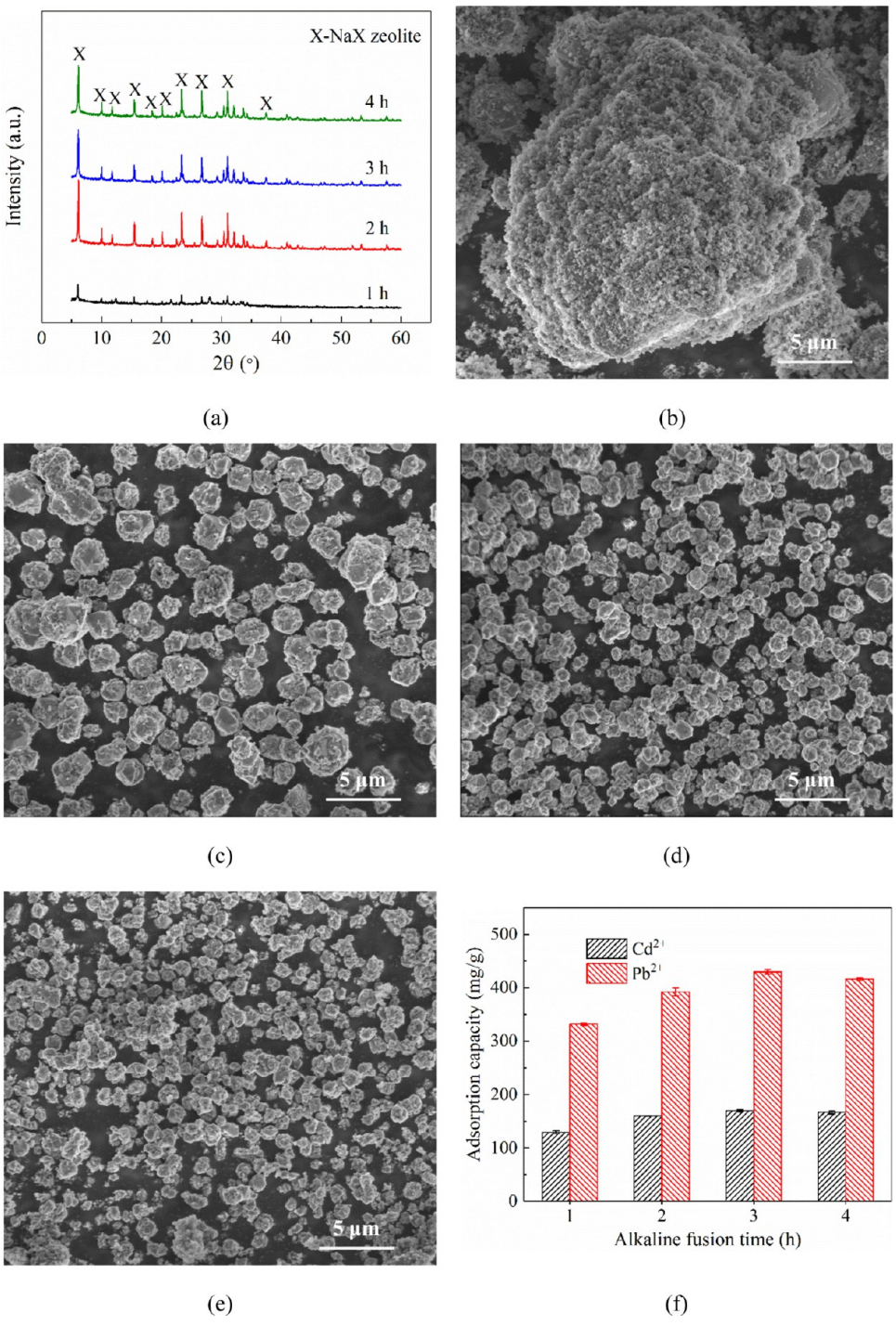

Figure 2. Impact of alkaline fusion time on the XRD pattern, SEM image and adsorption capacity of the synthesized product. (a) XRD patterns. (b–e) SEM images of the product derived from 1, 2, 3, and 4 h fusion. (f) adsorption capacity.

wide pore opening of 0.74 nm. These attributes render NaX zeolite highly effective for the adsorption of heavy metal ions.

3.1.2. Effect of Alkaline Fusion Time on Zeolite Synthesis. Figure 2 illustrates the effect of alkaline fusion time on the properties of the synthesized products. In Figure 2a, only faint diffraction peaks of NaX zeolite were observed in the product synthesized with a fusion time of 1 h, indicating that 1 h is insufficient for transforming coal gangue into an active phase, even at 800 °C. However, extending the fusion time to 2 h or more results in a significant increase in the intensity of these peaks, suggesting that a greater amount of NaX zeolite is produced from the coal gangue.

Figure 2b–e show that a short fusion time of 1 h predominantly results in large amorphous particles, consistent with the observed low crystallinity. In contrast, extending the fusion time to 2–4 h enhances crystallinity and yields smaller NaX particles. The crystal size is strongly influenced by the rate of nucleation and the growth rate of nuclei during the hydrothermal treatment.[30] SEM images further reveal that the crystal size decreases with increasing fusion time, suggesting

https://doi.org/10.1021/acsomega.4c07708
ACS Omega 2024, 9, 51237−51252

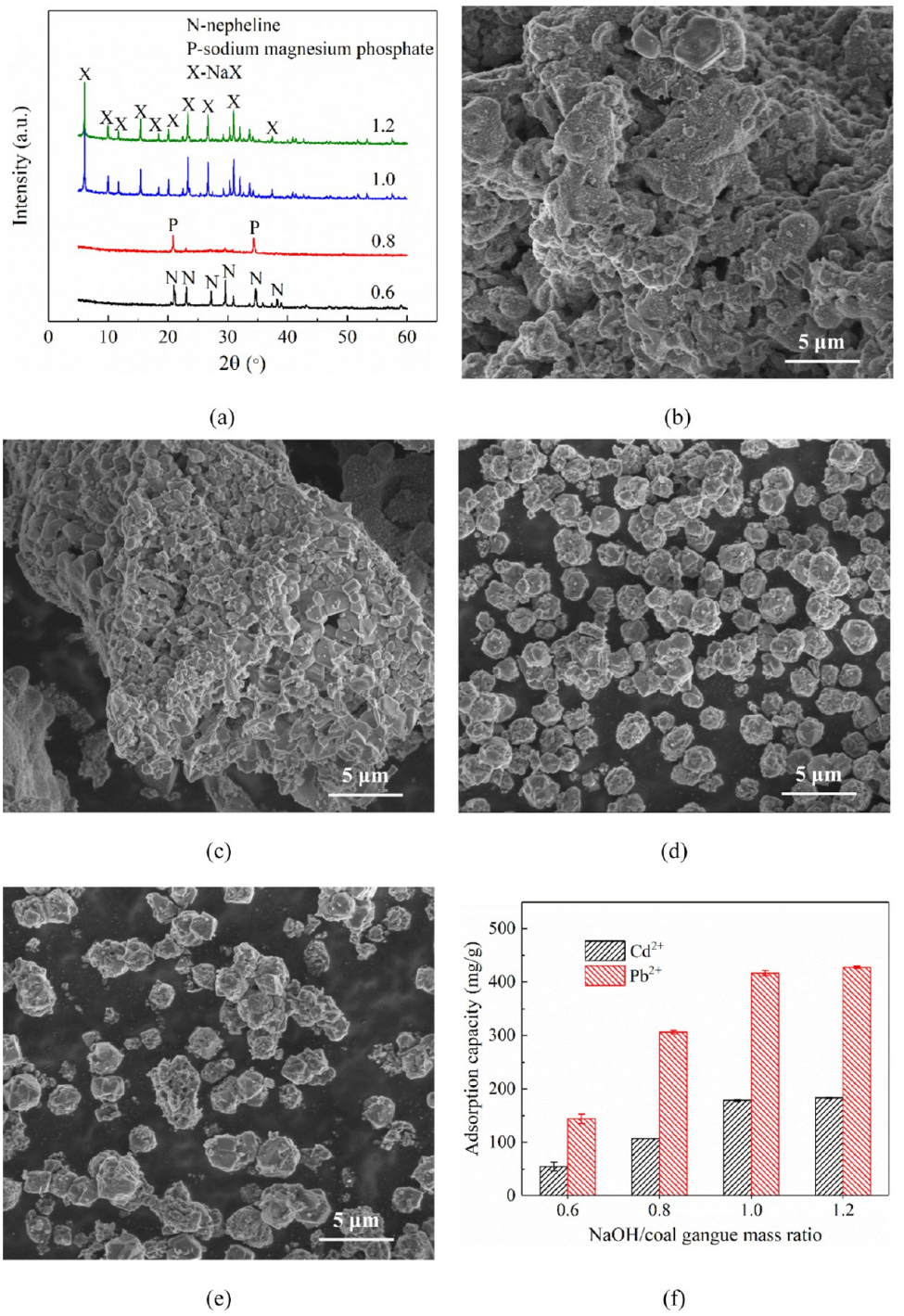

Figure 3. Impact of NaOH/coal gangue mass ratio on the XRD pattern, SEM image and adsorption capacity of the synthesized product. (a) XRD patterns. (b−e) SEM images of the product for the NaOH/coal gangue mass ratio of 0.6, 0.8, 1.0, and 1.2. (f) adsorption capacity.

that prolonged fusion leads to a greater generation of nuclei in the supersaturated solution.

Figure 2f demonstrates that as the fusion time increases from 1 to 3 h, both $q_{e,Cd}$ and $q_{e,Pb}$ rise from 129.4 and 332.0 to 166.9 and 416.1 mg/g, respectively. However, extending the fusion time to 4 h does not further enhance the adsorption capacity and even results in a decrease in $q_{e,Cd}$. These results suggest that excessively long fusion times may negatively impact adsorption performance. Therefore, a fusion time of 2−3 h is optimal for synthesizing NaX zeolite from the coal gangue used in this study.

3.1.3. Effect of NaOH Usage on Zeolite Synthesis. Figure 3 depicts the impact of NaOH usage on the characteristics of the synthesized products. Figure 3a indicates that at low NaOH/coal gangue mass ratios of 0.6 and 0.8, nepheline formed while no zeolite was generated. This outcome stems from insufficient NaOH, which fails to convert coal gangue into soluble aluminosilicate, a prerequisite for zeolite production from coal-based solid wastes. As the NaOH dosing amount increases, NaX zeolite can be synthesized at NaOH/coal gangue ratios of 1.0 and 1.2. However, excessive NaOH leads to the formation of stable zeolites like sodalite and cancrinite.[31]

https://doi.org/10.1021/acsomega.4c07708
ACS Omega 2024, 9, 51237−51252

Table 4. Analysis of Variance for $q_{e,Cd}$

source	sum of squares	degree of freedom	mean square	*F*-value	*P*-value	remarks
model	12 272.54	9	1363.62	42.77	<0.0001	highly significant
X_1-temperature	1031.22	1	1031.22	32.34	0.0007	significant
X_2-time	120.92	1	120.92	3.79	0.0925	not Significant
X_3-NaOH/coal gangue ratio	10 338.30	1	10 338.30	324.26	<0.0001	highly significant
X_1X_2	0.0292	1	0.0292	0.0009	0.9767	not Significant
X_1X_3	51.17	1	51.17	1.61	0.2457	not Significant
X_2X_3	17.06	1	17.06	0.5350	0.4883	not Significant
X_1^2	31.52	1	31.52	0.9885	0.3532	not Significant
X_2^2	29.12	1	29.12	0.9135	0.3710	not Significant
X_3^2	615.32	1	615.32	19.30	0.0032	significant
lack of fit	174.95	3	58.32	4.84	0.0810	not significant
pure error	48.23	4	12.06			
total	12 495.72	16				
R^2 = 0.9821	adj R^2 = 0.9592					

Table 5. Analysis of Variance for $q_{e,Pb}$

source	sum of squares	degree of freedom	mean square	*F*-value	*P*-value	remarks
model	54 344.59	9	6038.29	73.18	<0.0001	highly significant
X_1-temperature	16 186.37	1	16 186.37	196.18	<0.0001	highly significant
X_2-time	3440.73	1	3440.73	41.70	0.0003	significant
X_3-NaOH/coal gangue ratio	31 820.74	1	31 820.74	385.66	<0.0001	highly significant
X_1X_2	499.45	1	499.45	6.05	0.0434	significant
X_1X_3	69.44	1	69.44	0.8417	0.3894	not significant
X_2X_3	703.05	1	703.05	8.52	0.0224	significant
X_1^2	205.38	1	205.38	2.49	0.1586	not significant
X_2^2	331.87	1	331.87	4.02	0.0849	not significant
X_3^2	1172.89	1	1172.89	14.22	0.0070	significant
lack of fit	345.93	3	115.31	1.99	0.2576	not significant
pure error	231.63	4	57.91			
total	54 922.15	16				
R^2 = 0.9895	adj R^2 = 0.9760					

SEM images shown in Figure 3b−e are consistent with the XRD analysis results. When the NaOH/coal gangue mixing ratio is 0.6 or 0.8, the solid product primarily remains in an amorphous state due to insufficient OH^- ions provided by NaOH for effective activation and hydrothermal reaction of the coal gangue.[8] As the NaOH mixing ratio increases to 1.0 and 1.2, the amorphous phase is eliminated, and small NaX crystals begin to form.

Figure 3f shows a significant increase in $q_{e,Cd}$ and $q_{e,Pb}$ from 55.1 and 144.2 mg/g to 178.7 and 416.9 mg/g, respectively, as the NaOH/coal gangue ratio increases from 0.6 to 1.0. Further increasing the ratio to 1.2 results in minimal changes in $q_{e,Cd}$ and $q_{e,Pb}$. Therefore, a NaOH/coal gangue ratio of 1.0 is considered optimal for zeolite production in this study.

3.2. Optimization of Reaction Conditions by RSM.

3.2.1. RSM Model Fitting. The 17 experimental runs suggested by the Box-Behnken method were conducted, and the adsorption results are presented in Table 3. Using RSM analysis, predictions for $q_{e,Cd}$ and $q_{e,Pb}$ were generated with fitted second-order polynomial regression models, known as quadratic models. The RSM models established for $q_{e,Cd}$ and $q_{e,Pb}$ are represented by Formulas 3 and 4, respectively.

$$q_{e,Cd} = -481.86 + 0.315X_1 + 29.39X_2 + 689.97X_3 + 0.000855X_1X_2 + 0.179X_1X_3 - 10.33X_2X_3 - 0.000274X_1^2 - 2.63X_2^2 - 302.22X_3^2 \quad (3)$$

$$q_{e,Pb} = -929.32 + 0.0156X_1 + 111.98X_2 + 1494.54X_3 - 0.112X_1X_2 - 0.208X_1X_3 - 66.29X_2X_3 + 0.000698X_1^2 + 8.88X_2^2 - 417.25X_3^2 \quad (4)$$

3.2.2. ANOVA Tests. Analysis of variance (ANOVA) was performed to evaluate the statistical significance and adequacy of the model equations, along with the individual and interactive effects of the variables on the response values. The comprehensive results are provided in Tables 4 and 5 for $q_{e,Cd}$ and $q_{e,Pb}$, respectively. The findings from ANOVA demonstrate that the models exhibit high significance at the 95% confidence level, as evidenced by high *F*-values (42.77 for $q_{e,Cd}$ and 73.18 for $q_{e,Pb}$) and very low *P*-values (<0.0001). The *P*-value reflects the probability of error and is crucial for determining the significance of each regression coefficient. Variables with $P < 0.05$ are generally considered significant, with *P* values <0.0001 indicating exceptionally significant effects. For $q_{e,Cd}$, the variables X_1, X_3, and X_3^2 demonstrate significant effects, whereas for $q_{e,Pb}$, variables X_1, X_2, X_3, X_1X_2, X_2X_3, and X_3^2 are significant. Notably, the NaOH/coal gangue weight ratio (X_3) emerges as the most influential variable in the production of heavy metal adsorbents from coal gangue, as indicated by its exceptionally high *F*-values (324.26 for $q_{e,Cd}$ and 385.66 for $q_{e,Pb}$) and very low *P*-values (<0.0001).

Tables 4 and 5 further illustrate that the Lack of Fit *F*-values for both $q_{e,Cd}$ and $q_{e,Pb}$ are well below 0.05, indicating a strong

https://doi.org/10.1021/acsomega.4c07708
ACS Omega 2024, 9, 51237−51252

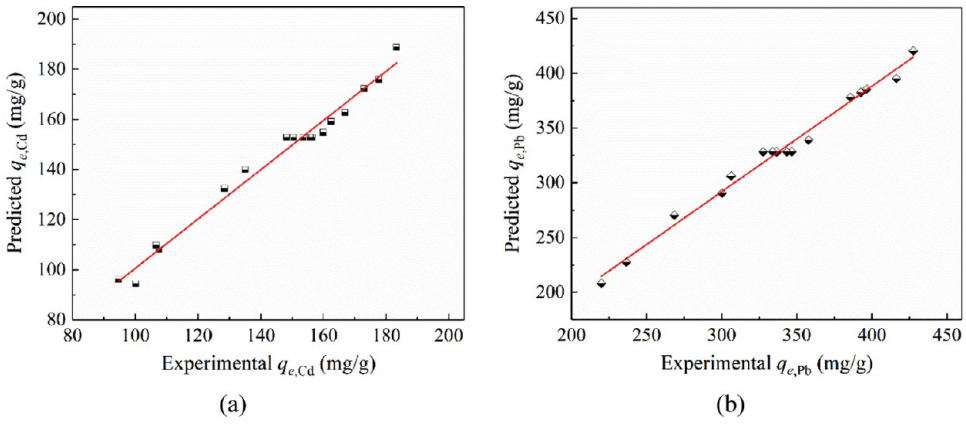

Figure 4. Predicted versus experimental adsorption capacity values. (a) $q_{e,Cd}$ values. (b) $q_{e,Pb}$ values.

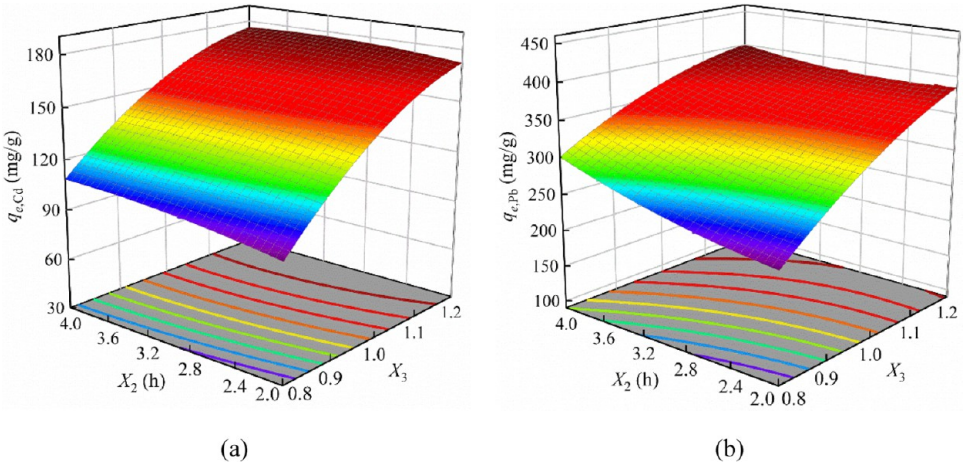

Figure 5. Combined effects of fusion time (X_2) and NaOH/coal gangue ratio (X_3) on the adsorption capacity. (a) $q_{e,Cd}$. (b) $q_{e,Pb}$.

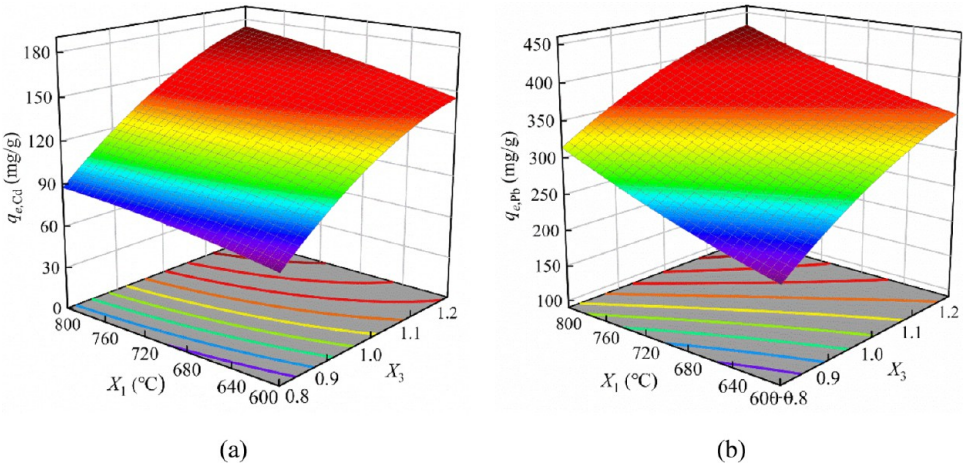

Figure 6. Combined effects of fusion temperature (X_1) and NaOH/coal gangue ratio (X_3) on the adsorption capacity. (a) $q_{e,Cd}$. (b) $q_{e,Pb}$.

fit between the quadratic models and the experimental data. The model fitness was further evaluated using the coefficient of determination (R^2), which yielded values of 98% for both $q_{e,Cd}$ and $q_{e,Pb}$, highlighting the high accuracy of these models. Figure 4 shows the predictive accuracy of the model by comparing experimental and predicted adsorption capacities. The data points closely follow the straight line, demonstrating excellent agreement between experimental observations and model predictions. In conclusion, the models effectively capture the experimental relationships between variables and responses, validating their suitability for this study.

3.2.3. Variables Interactions Analysis. Figure 5 illustrates the relationship between alkaline fusion time and the NaOH/coal gangue ratio while keeping the fusion temperature constant at 700 °C. The figure demonstrates that increasing the NaOH/coal gangue ratio positively affects the adsorption capacity of heavy metal ions, regardless of whether the fusion time is short or long. For example, raising the NaOH/coal

https://doi.org/10.1021/acsomega.4c07708
ACS Omega 2024, 9, 51237−51252

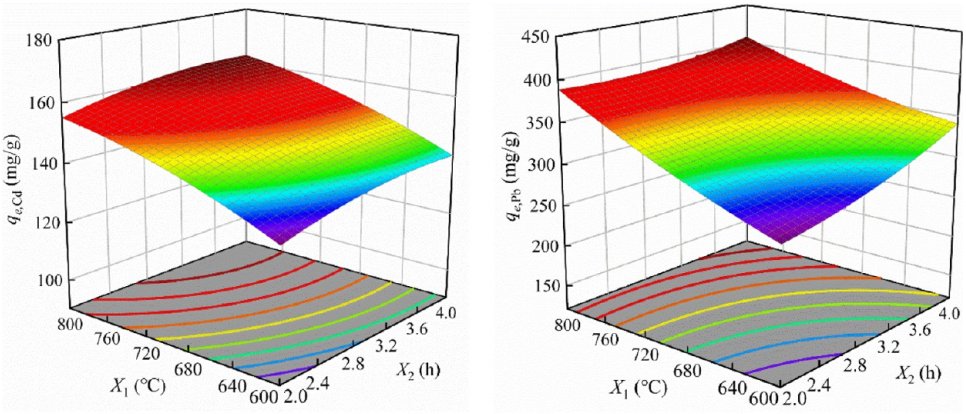

Figure 7. Combined effects of fusion temperature (X_1) and fusion time (X_2) on the adsorption capacity. (a) $q_{e,Cd}$. (b) $q_{e,Pb}$.

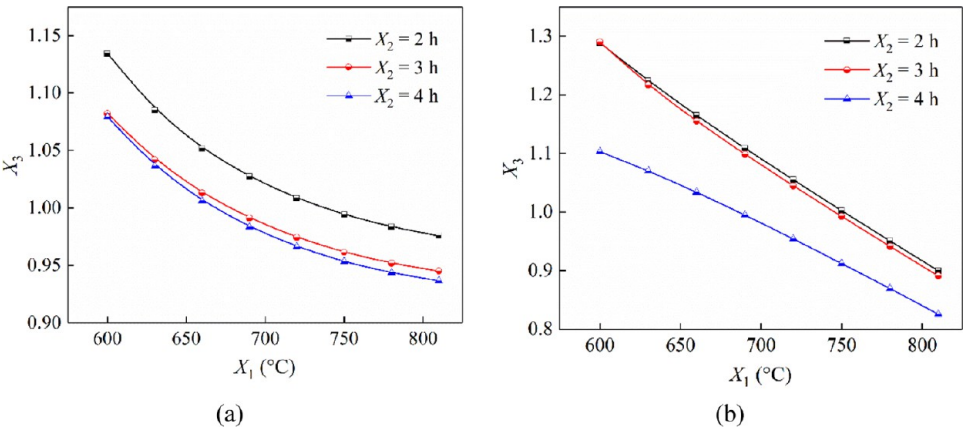

Figure 8. Relationship between alkaline fusion temperature (X_1) and NaOH/coal gangue ratio (X_3) at a given adsorption capacity. (a) Cd^{2+}. (b) Pb^{2+}.

gangue ratio from 0.8 to 1.2 results in an increase in $q_{e,Cd}$ from 96.1 to 172.2 mg/g at a fusion time of 2 h, and from 108.0 to 175.8 mg/g at a fusion time of 4 h. In contrast, the fusion time has minimal impact on $q_{e,Cd}$ and only a slight effect on $q_{e,Pb}$ at lower NaOH/coal gangue ratios. Since extended alkaline fusion times result in high energy consumption, increasing the fusion duration is not an effective approach for enhancing adsorption performance.

Figure 6 illustrates the interaction between fusion temperature and the NaOH/coal gangue ratio, with the fusion time held constant at 3 h. The NaOH/coal gangue ratio has a more pronounced effect on $q_{e,Cd}$ compared to fusion temperature. For example, at a NaOH/coal gangue ratio of 0.8 and a fusion temperature of 600 °C, the $q_{e,Cd}$ value is 94.2 mg/g. Increasing the NaOH/coal gangue ratio to 1.2 raises this value to 159.0 mg/g, while increasing the fusion temperature to 700 °C only increases it to 104.7 mg/g. In contrast, both the NaOH/coal gangue ratio and fusion temperature have a similar impact on the Pb^{2+} adsorption capacity. Increasing the amount of alkali dosing can reduce the required alkaline fusion temperature, which in turn lowers both energy consumption and processing costs. Some researchers have also utilized Na_2CO_3 alongside NaOH to activate coal gangue.[32−34] Consequently, using low-cost alkalis, such as natural trona, represents a promising method for enhancing the economic feasibility of zeolitization processes.

Figure 7 illustrates the interaction between fusion temperature and fusion time, with the NaOH/coal gangue ratio fixed at 1.0. Within the range of fusion temperatures studied, increasing the fusion time does not lead to a significant improvement in $q_{e,Cd}$ and $q_{e,Pb}$. Across fusion times ranging from 2 to 4 h, higher fusion temperatures generally enhance the performance of heavy metal adsorption, underscoring the importance of elevated fusion temperatures. High-temperature alkaline fusion is a crucial process that significantly impacts the production cost of zeolites. To optimize zeolitization processes, alternative energy sources such as ultrasound and microwave irradiation should be explored.[6] For example, Li et al.[35] created an analcime-activated carbon composite through a microwave-assisted hydrothermal technique utilizing coal gangue, thereby bypassing the requirements for calcination or alkaline-fusion melting.

3.2.4. Validation and Application. The optimal condition for Cd^{2+} adsorption was found to be a fusion temperature of 796 °C, a fusion time of 2.7 h and a NaOH/coal gangue weight ratio of 1.2. The predicted maximum $q_{e,Cd}$ under these conditions is 187.5 mg/g. For Pb^{2+} adsorption, the optimal condition is a fusion temperature of 794 °C, a fusion time of 2.8 h and a NaOH/coal gangue weight ratio of 1.2, with a predicted $q_{e,Pb}$ of 427.6 mg/g. To validate these predictions, experiments were conducted under these optimized conditions, resulting in experimental $q_{e,Cd}$ of 181.3 mg/g and

https://doi.org/10.1021/acsomega.4c07708
ACS Omega 2024, 9, 51237−51252

Table 6. Kinetics Parameters for Cd^{2+} and Pb^{2+} Adsorption by the NaX Sample

		pseudo-first-order model			pseudo-second-order model		
ion	experimental q_e (mg/g)	k_1	R^2	calculated q_e (mg/g)	k_2 ($\times 10^{-4}$)	R^2	calculated q_e (mg/g)
Cd^{2+}	158.1	0.0060	0.959	47.2	5.41	0.999	159.2
Pb^{2+}	430.4	0.0069	0.978	145.6	1.74	0.999	434.8

experimental $q_{e,Pb}$ of 419.9 mg/g. These experimental values closely aligned with the predicted values obtained from the regression model.

Based on the above discussion, the fusion time was determined to be a nonsignificant factor affecting adsorption capacity within the 2−4 h range. The RSM models were used to analyze the relationship between fusion temperature and the NaOH/coal gangue ratio for a given adsorption capacity. Figure 8 illustrates that, for target adsorption capacities of 150 mg/g for $q_{e,Cd}$ and 350 mg/g for $q_{e,Pb}$, the NaOH/coal gangue ratio decreases as the fusion temperature increases. For example, with the alkaline fusion time fixed at 2 h, increasing the NaOH/coal gangue weight ratio from 0.976 to 1.134 and from 0.900 to 1.289 enables a reduction in alkaline fusion temperature from 800 to 600 °C. This implies that to achieve the desired adsorption capacity, one can either reduce the NaOH usage by increasing the fusion temperature or decrease the fusion temperature by increasing the NaOH usage. The RSM models are useful for economic analysis of zeolite synthesis, highlighting the importance of optimizing the use of low-cost heat sources and alkaline mediums to enhance economic viability.

3.3. Adsorption Characteristics. As the NaX-800, 3, 1.2 sample has the best adsorption performance, it was selected to explore the adsorption characteristics.

3.3.1. Adsorption Kinetics. Figure S1 illustrates the adsorption profiles of heavy metal ions over varying time periods. Both Cd^{2+} and Pb^{2+} ions show a significant increase in adsorption during the first 360 min, followed by a gradual approach to equilibrium by 1440 min. The pseudo-first-order and pseudo-second-order models were commonly employed across various adsorption systems. The linear representation of the pseudo-first-order kinetics is given by Formula 5.

$$\ln(q_e - q_t) = \ln q_e - k_1 t \tag{5}$$

where k_1 represents the rate constant for the pseudo-first-order model (1/min). The values of q_e and k_1 are obtained from the slope and intercept of the linear plot of $\ln(q_e - q_t)$ versus t, respectively. The linear form of the pseudo-second-order model is expressed by Formula 6.

$$\frac{t}{q_t} = \frac{1}{k_2 q_e^2} + \frac{t}{q_e} \tag{6}$$

where k_2 denotes the rate constant for the pseudo-second-order model (g/(mg·min)). The values of q_e and k_2 are derived from the slope and intercept of the plot of t/q_t versus t, respectively. Figure S2 presents the kinetic fitting for the adsorption of Cd^{2+} and Pb^{2+} onto the modified CG samples.

As shown in Table 6, the high correlation coefficients and the close alignment between the calculated q_e values and the experimental q_e values indicate that the pseudo-second-order model effectively describes the adsorption kinetics of Cd^{2+} and Pb^{2+} on NaX-800, 3, 1.2. These results are in agreement with findings from other studies.[7,8,12] The pseudo-second-order model encompasses both the diffusion process and the surface reaction process, implying that the surface adsorption is the rate-limiting step, which is affected by the availability of adsorption sites.

3.3.2. Adsorption Isotherms. To elucidate the adsorption mechanism and ascertain the maximum adsorption capacity, it is crucial to examine the adsorption isotherm. As depicted in Figure S3, the adsorption capacity for Cd^{2+} and Pb^{2+} initially rises sharply with increasing initial concentration, followed by a more gradual increase across the tested concentration range. The experimental data were analyzed using two widely recognized isotherm models: the Langmuir and Freundlich models. The linear form of the Langmuir equation is expressed by Formula 7.

$$\frac{c_e}{q_e} = \frac{1}{K_L q_m} + \frac{c_e}{q_m} \tag{7}$$

where c_e represents the equilibrium concentration of the metal ion in solution (mg/L), while q_m denotes the maximum metal ion uptake per unit mass of the adsorbent (mg/g). K_L is the Langmuir constant which relates to the adsorption rate (L/mg). To determine q_m and K_L, one can plot c_e/q_e against c_e, which yields a straight line with a slope of $1/q_m$ and an intercept of $1/(K_L q_m)$. The Freundlich model is formulated as Formula 8.

$$\ln q_e = \ln K_F + \frac{1}{n} \ln c_e \tag{8}$$

where K_F serves as an approximate indicator of the adsorption capacity ((mg/g)/(mg/L)$^{1/n}$), while $1/n$ reflects the adsorption intensity of the metal ion on the synthesized zeolite NaX. By plotting $\ln q_e$ against $\ln c_e$, the values of $1/n$ and K_F can be determined from the slope and intercept of the resulting graph. The fitting results for the adsorption of Cd^{2+} and Pb^{2+} onto the NaX-800, 3, 1.2 sample are illustrated in Figure S4 and summarized in Table 7.

Table 7. Parameters of the Adsorption Isotherm Models

	Langmuir model			Freundlich model		
ion	q_m (mg/g)	K_L (L/mg)	R^2	K_F (mg/g)/(mg/L)$^{1/n}$	$1/n$	R^2
Cd^{2+}	194.6	0.3117	0.990	97.0	0.148	0.777
Pb^{2+}	546.5	0.0733	0.972	116.4	0.302	0.756

For both Cd^{2+} and Pb^{2+} adsorption, the coefficient values of determination for the Langmuir model significantly exceed those of the Freundlich model, suggesting that the Langmuir model more accurately describes the adsorption process, indicative of monolayer adsorption on the NaX-800, 3, 1.2 surface. Previous studies have similarly indicated that the adsorption of heavy metal ions by zeolite materials aligns more closely with the Langmuir model.[7,8] In the Langmuir model, the equilibrium analysis coefficient R_L (calculated as $R_L = 1/(1 + K_L \cdot q_m)$) serves to estimate the adsorption affinity and can be derived from the fitting results presented in Table 7. The

https://doi.org/10.1021/acsomega.4c07708
ACS Omega 2024, 9, 51237−51252

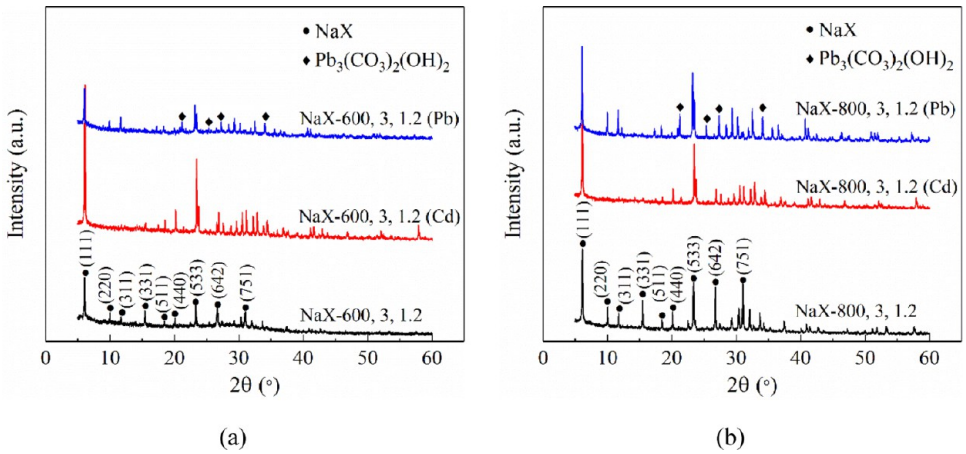

Figure 9. XRD patterns of the synthesized NaX samples before and after adsorption. (a) NaX-600, 3, 1.2. (b) NaX-800, 3, 1.2.

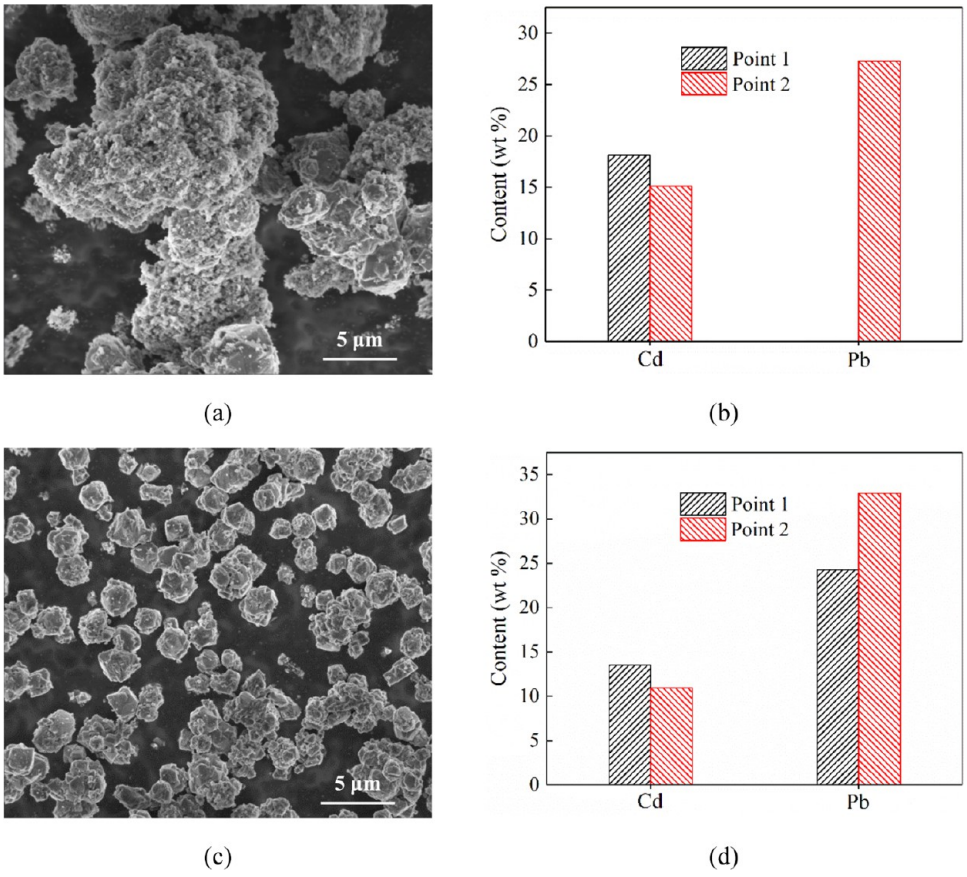

Figure 10. SEM image and EDS analysis results of NaX before and after adsorption. (a) NaX-600, 3, 1.2. (b) EDS analysis results of NaX-600, 3, 1.2 after adsorption. (c) NaX-800, 3, 1.2. (d) EDS analysis results of NaX-800, 3, 1.2 after adsorption.

values of R_L can be interpreted as follows: (1) favorable adsorption when $0 < R_L < 1$; (2) unfavorable adsorption when $R_L > 1$; (3) linear adsorption when $R_L = 1$; and (4) irreversible adsorption when $R_L = 0$.[36] The calculated R_L values for Cd^{2+} and Pb^{2+} were 0.016 and 0.024, respectively, indicating favorable adsorption as both values fall within the range of 0−1. Additionally, the Freundlich equation parameter $1/n$ can be categorized into five zones: $1/n < 0.01$, $0.01 < 1/n < 0.1$, $0.1 < 1/n < 0.5$, $0.5 < 1/n < 1$, and $1/n > 1$.[37] For the Freundlich model, the $1/n$ values for Cd^{2+} and Pb^{2+} were determined to be 0.148 and 0.302, respectively. These values suggest that the adsorption process by NaX-800, 3, 1.2 is characterized by preferential adsorption with a strong affinity, which aligns with findings from other studies.[7,12]

3.3.3. Effect of Initial pH and Adsorbent Dosage. Figure S5 illustrates the impact of adsorbent dosage on adsorption performance. The removal efficiency of NaX-800, 3, 1.2 for Cd^{2+} increased from 23.5 to 99.3% as the adsorbent dosage rose from 0.1 to 1 g/L, while the removal efficiency for Pb^{2+} increased from 48.0 to 96.8% with an increase in dosage from 0.1 to 0.3 g/L. These improvements were attributed to the increased availability of adsorption sites. However, a higher adsorbent dosage led to a decrease in the adsorption capacity of NaX-800, 3, 1.2 for both Cd^{2+} and Pb^{2+}, which can be

https://doi.org/10.1021/acsomega.4c07708
ACS Omega 2024, 9, 51237−51252

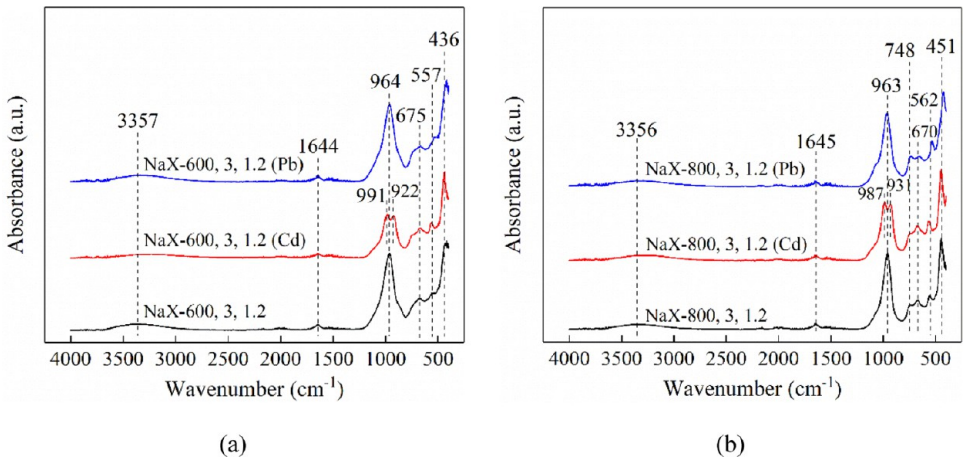

Figure 11. FTIR spectra of NaX before and after adsorption. (a) NaX-600, 3, 1.2. (b) NaX-800, 3, 1.2.

ascribed to the agglomeration of adsorbent particles. Similar findings have been reported in the literature.[9]

The initial pH is a critical parameter influencing the adsorption of heavy metal ions by NaX zeolite. Figure S6 presents the changes in the q_e values of NaX-800, 3, 1.2 for Cd^{2+} and Pb^{2+} across a pH range of 2−7. The adsorption capacity increased with rising pH within the studied range. This phenomenon can be attributed to the competition between H^+ ions and positively charged heavy metal ions. Ion exchange has been recognized as a significant mechanism for the removal of heavy metal ions by zeolite materials.[9] In strongly acidic conditions, abundant H^+ ions compete with heavy metal ions for active ion exchange sites on the zeolite surface, resulting in lower adsorption capacity. As the pH increases, the competitive effect diminishes, thereby enhancing both adsorption efficiency and capacity. Additionally, the formation of metal complexes at higher pH levels also contributes to improved adsorption performance.[12]

3.4. Adsorption Mechanism. To gain deeper insights into the adsorption mechanisms of NaX zeolite, NaX-600, 3, 1.2 and NaX-800, 3, 1.2 were characterized before and after the adsorption of Cd^{2+} and Pb^{2+} using XRD, SEM-EDS, FTIR, XPS and N_2 adsorption−desorption isotherms. The samples are designated as follows: NaX-600, 3, 1.2 (Cd) and NaX-600, 3, 1.2 (Pb) for the NaX-600, 3, 1.2 after the adsorption of Cd^{2+} and Pb^{2+}, respectively. Similarly, NaX-800, 3, 1.2 (Cd) and NaX-800, 3, 1.2 (Pb) refer to the NaX-800, 3, 1.2 subjected to the same adsorption processes.

3.4.1. XRD. Figure 9 shows that the XRD patterns of NaX samples before and after the adsorption of Cd^{2+} and Pb^{2+} are quite similar, indicating that the overall zeolite structure is not significantly altered by the adsorption processes. However, some minor variations are observed in the XRD patterns following adsorption. Specifically, the peaks corresponding to the (2 2 0) and (3 1 1) lattice planes disappear after Cd^{2+} adsorption, and the intensity ratio I(2 2 0)/I(3 1 1) decreases after Pb^{2+} adsorption. This intensity ratio reflects changes in the distribution of Na^+ ions within the supercages, indicating a shift from random positions to specific sites due to the incorporation of larger ions.[9,38] The observed changes in the I(2 2 0) and I(3 1 1) peaks suggest that Cd^{2+} and Pb^{2+} adsorption occurs via cation exchange. Additionally, hydrocerussite ($Pb_3(CO_3)_2(OH)_2$) was detected in the NaX samples after Pb^{2+} adsorption, indicating that Pb^{2+} can also be retained in the NaX structure through precipitation. Lyu et al.[39] also observed the formation of $Pb_3(CO_3)_2(OH)_2$ in the removal of Pb^{2+} by modified red mud and proposed two possible pathways.

3.4.2. SEM-EDS. Figure 10 presents SEM images and EDS analysis results of NaX following the adsorption of heavy metal ions. No significant changes in morphology are observed in the NaX samples following the adsorption of Cd^{2+} and Pb^{2+}. Although EDS analysis only provides semiquantitative results, Figures 10b,10d indicate that Cd^{2+} is distributed more uniformly across the NaX surface, with Cd^{2+} content at two random positions showing closely matching values. This observation suggests that Cd^{2+} preferentially remains on the surface of NaX crystals. In contrast, Pb^{2+} seems to be distributed more unevenly across the NaX surface. This uneven distribution may be attributed to the formation of $Pb_3(CO_3)_2(OH)_2$, a compound that tends to adhere nonuniformly to the pore surfaces. Figures S7 and S8 display the energy dispersive spectra for NaX-600, 3, 1.2 and NaX-800, 3, 1.2, respectively, after adsorption of Cd^{2+} and Pb^{2+}.

3.4.3. FTIR. Figure 11 presents the FTIR spectra of synthesized NaX zeolite before and after the adsorption of Cd^{2+} and Pb^{2+} ions. The peak around 3437 cm^{-1} corresponds to the stretching vibration of H−O bonds, while the peak at 1645 cm^{-1} is attributed to the bending vibration of absorbed water in the zeolite. The bands at 963 cm^{-1} (asymmetric stretching) and 748 cm^{-1} (symmetric stretching vibrations of Si−O−Si or Si−O−Al bridges) are associated with the internal vibrations of Si−O−Al. Additionally, the peak at 451 cm^{-1} indicates the bending vibration of Si−O−Al bonds, suggesting the bridging of [SiO_4] and [AlO_4] tetrahedra by an oxygen atom. The band at 562 cm^{-1} is attributed to the double six-membered rings (D6R) that connect the β-cage.[9] Notably, compared to the raw NaX zeolite, the characteristic peaks of the zeolite after Pb^{2+} adsorption remained largely unchanged. However, after Cd^{2+} adsorption, the peak at 963 cm^{-1} splited into two lower peaks. The presence of nontetrahedral cations can alter the IR spectra of zeolite frameworks depending on factors such as mass, charge, ion size and the cation's environment.[40] Generally, hydrated cations tend to occupy the supercage or β-cage of faujasite-like zeolites such as NaX and NaY.[9] Given that hydrated Cd^{2+} (0.43 nm) is slightly larger than hydrated Pb^{2+} (0.4 nm), Cd^{2+} may occupy different positions within the pore channels compared to Pb^{2+}, thereby exerting a more pronounced effect on the structure of the silicon−oxygen and aluminum−oxygen tetrahedra.

https://doi.org/10.1021/acsomega.4c07708
ACS Omega 2024, 9, 51237−51252

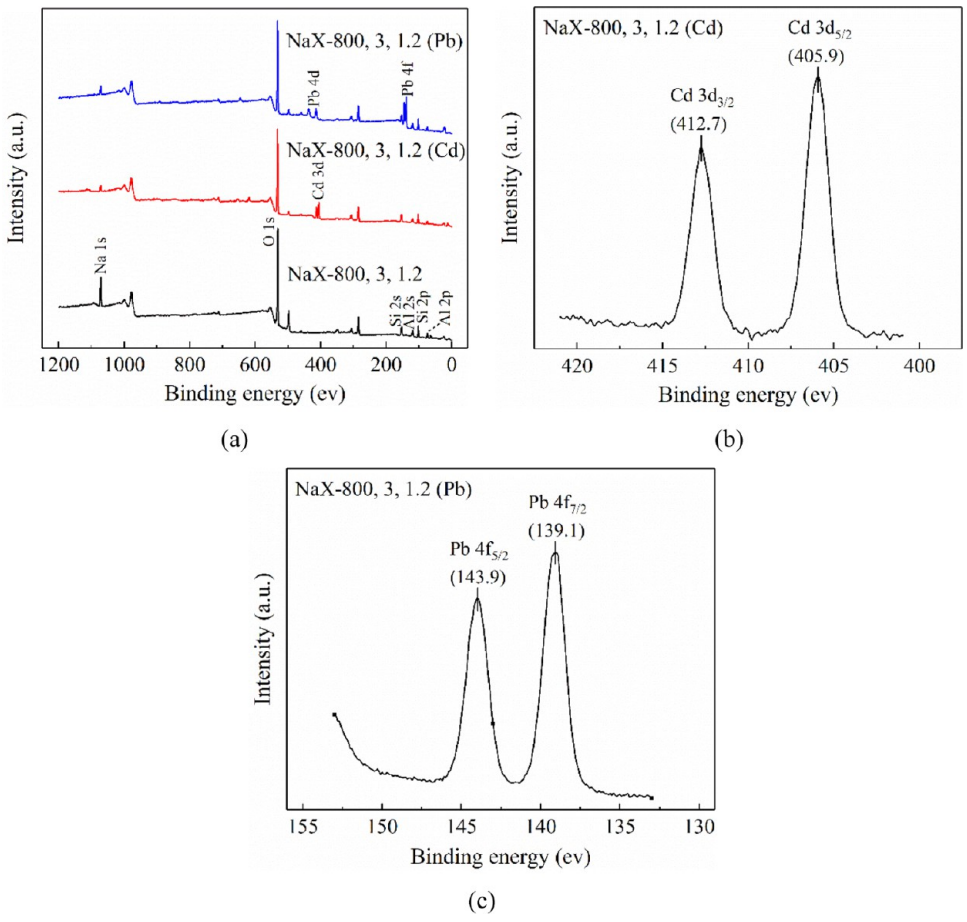

Figure 12. XPS results of the NaX-800, 3, 1.2 before and after the adsorption of Cd^{2+} and Pb^{2+}. (a) full spectrum. (b) Cd 3d; (c) Pb 4f.

Table 8. Pore Structure Parameters of NaX Zeolite Samples before and after Adsorption

sample	S_{BET} (m^2/g)[a]	S_{micro} (m^2/g)[b]	S_{ext} (m^2/g)[c]	V_{total} (cm^3/g)[d]	V_{micro} (cm^3/g)[b]	D_{pore} (nm)[e]
NaX-800, 3, 1.2	734.71	596.46	138.24	0.349	0.226	3.41
NaX-800, 3, 1.2 (Cd)	612.44	433.49	178.95	0.327	0.169	4.31
NaX-800, 3, 1.2 (Pb)	316.83	197.90	118.93	0.225	0.079	4.95

[a]Determined by multipoint BET method. [b]Measured by the *t*-plot method. [c]Calculated by difference. [d]Calculated from absorbed volume of N_2 at a relative pressure P/P_0 of 0.99. [e]Determined by BJH method using the adsorption branches of N_2 isotherms.

3.4.4. XPS Analysis. Figure 12 presents the XPS analysis results of the synthesized NaX before and after the adsorption of Cd^{2+} and Pb^{2+}. The full spectrum shown in Figure 12a indicates that the binding energies of Na 1s, O 1s, Si 2p, and Al 2p for NaX-800, 3, 1.2 are consistent with values reported in the literature.[9,41] Figure 12b confirms the adsorption of Cd^{2+} on NaX-800, 3, 1.2, as evidenced by the emergence of two peaks at 405.9 and 412.7 eV, which correspond to Cd $3d_{5/2}$ and Cd $3d_{3/2}$, respectively. Similarly, Figure 12c confirms the adsorption of Pb^{2+} on NaX-800, 3, 1.2, indicated by the appearance of two peaks at 139.1 and 143.9 eV, characteristic of Pb $4f_{7/2}$ and Pb $4f_{5/2}$, respectively. Notably, the Na 1s peaks in NaX-800, 3, 1.2 (Cd) and NaX-800, 3, 1.2 (Pb) are significantly diminished compared to those in NaX-800, 3, 1.2, suggesting that ion exchange occurs between the heavy metal ions and Na^+ ions during the process. These XPS results are consistent with the XRD findings.

3.4.5. N_2 Adsorption−Desorption Analysis. Figure S9 illustrates the nitrogen adsorption−desorption isotherms for the NaX-800, 3, 1.2 zeolite before and after adsorption. All samples display a typical Type I adsorption isotherm, characteristic of microporous materials, with a significant uptake observed at low P/P_0 values. The presence of a small hysteresis loop at relative pressures between 0.4 and 0.99 P/P_0 is likely due to intercrystalline pores created by the stacking of NaX particles. Table 8 summarizes the pore structure parameters of the NaX samples, which are consistent with values reported in the literature. Adsorption of both Cd^{2+} and Pb^{2+} resulted in a reduction in the total surface area (S_{BET}) and total pore volume (V_{total}) of the NaX samples, with Pb^{2+} adsorption exerting a more pronounced effect. The S_{BET} of NaX-800, 3, 1.2 decreased from 734.71 to 612.44 and 316.83 m^2/g following Cd^{2+} and Pb^{2+} adsorption, respectively. These reductions are attributed to the incorporation of Cd^{2+} and Pb^{2+} into the pore channels of NaX. The higher adsorption capacity for Pb^{2+} compared to Cd^{2+} suggests that more pores were occupied following Pb^{2+} adsorption.

Table 8 also shows that the decrease in S_{BET} after Pb^{2+} adsorption is primarily attributed to a reduction in the micropore surface area (S_{micro}). In contrast, Cd^{2+} adsorption

https://doi.org/10.1021/acsomega.4c07708
ACS Omega 2024, 9, 51237−51252

increased the external surface area (S_{ext}) while decreasing both S_{BET} and S_{micro}. For the synthesized NaX samples, it is suggested that micropores are predominantly located within the NaX crystals, while external pores primarily result from the stacking of NaX crystals. The variation in pore parameters can be explained by the fact that hydrated Pb^{2+}, with a smaller kinetic radius (0.4 nm), is able to enter the micropore system more effectively. In comparison, the larger hydrated Cd^{2+} (0.43 nm) tends to be trapped on the surface of NaX crystals, potentially creating additional external pores by altering the contact between NaX crystals.

3.5. Stabilization Performance of NaX Zeolite for Cd in the Soil. Figure 13 illustrates the distribution of Cd in the contaminated soil before and after remediation with NaX. In the raw soil, Cd was primarily found in the form of Fe−Mn oxides (12.93 mg/kg) and carbonates (6.42 mg/kg), with a smaller amount present in the exchangeable form (3.51 mg/kg). Only trace amounts of Cd were found in the organic matter and residual forms (<0.5 mg/kg). The exchangeable form, which is more mobile in a neutral environment, poses a greater risk to vegetation and the surrounding environment. After 3 weeks of incubation with NaX-600, 3, 1.2 and NaX-800, 3, 1.2, the exchangeable fraction of Cd decreased to 2.79 and 1.36 mg/kg, respectively. Simultaneously, there was a notable increase in the Cd content in the carbonate and Fe−Mn oxide fractions. Carbonate-bound Cd tends to be more harmful in acidic environments, while Fe−Mn oxide-bound Cd is more significant under reducing conditions.[27] The observed changes in Cd distribution suggest that NaX is effective in immobilizing Cd in the soil.

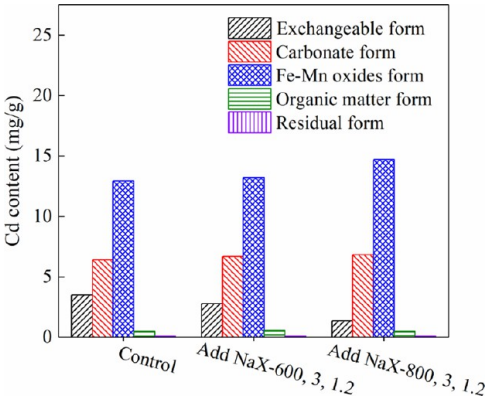

Figure 13. Distribution of Cd in the contaminated soil before and after NaX remediation.

In the remediation of heavy metal-polluted soil, enhancing the binding strength between NaX and heavy metal ions is crucial, in addition to increasing NaX's adsorption capacity. This ensures that heavy metal ions adhere firmly to NaX and are less likely to desorb into the surrounding environment. Ion exchange is the primary mechanism for Cd adsorption by NaX. Within the zeolite's pore structure, each aluminum−oxygen tetrahedron carries a negative charge that must be neutralized by cations. Since cation exchange sites are primarily associated with aluminum−oxygen tetrahedra, an effective strategy to enhance adsorption performance may involve adding an additional aluminum source to create more adsorption sites. It has been reported that, with increasing Si/Al ratio in the reaction mixture, the zeolite type transitions from NaA to NaX and then to NaY.[42,43] Therefore, the optimal Si/Al ratio should be determined by comparing the adsorption performance of these different types of zeolites. Additionally, the pore structure of zeolites significantly impacts the adsorption process. A hierarchical pore system is generally considered more advantageous for heavy metal adsorption. For example, Bu et al.[14] developed a consecutive alkaline and ultrasonic post-treatment method, which will lead to the formation of hierarchical mesopores and improve the adsorption performance of mesoporous zeolites. In summary, optimizing the adsorption performance of zeolite derived from coal gangue involves controlling both its adsorption sites and pore structure. This will be a central focus of our future research.

4. CONCLUSIONS

This study synthesized NaX zeolite from coal gangue and evaluated its efficacy in remediating Cd and Pb contamination in both water and soil. The synthesis parameters, including alkaline fusion temperature, duration and the NaOH/coal gangue weight ratio, were optimized using RSM. Adsorption mechanisms were elucidated through various techniques, including XRD, SEM-EDS, FTIR, XPS and nitrogen adsorption−desorption techniques. The key findings are as follows:

(1) The optimal synthesis conditions for NaX zeolite were found to be an alkaline fusion temperature of approximately 800 °C, a duration of about 2.8 h and a NaOH/coal gangue weight ratio of 1.2. The maximum adsorption capacities for Cd^{2+} and Pb^{2+} are 181.3 and 419.9 mg/g, respectively. The NaOH/coal gangue weight ratio was identified as the most significant factor influencing adsorption performance.

(2) RSM models reveal that increasing the NaOH/coal gangue weight ratio allows for a reduction in the alkaline fusion temperature. For target adsorption capacities of 150 mg/g for Cd^{2+} and 350 mg/g for Pb^{2+}, maintaining an alkaline fusion duration of 2 h, increasing the NaOH/coal gangue weight ratio from 0.976 to 1.134 and from 0.900 to 1.289 enables a reduction in alkaline fusion temperature from 800 to 600 °C.

(3) NaX zeolite primarily removes Cd^{2+} and Pb^{2+} through ion exchange, with these ions entering the zeolite's cage-like structure. Pb^{2+} may also precipitate as hydrocerussite ($Pb_3(CO_3)_2(OH)_2$) within the zeolite channels. Cd^{2+} appears to interact differently within the pore channels compared to Pb^{2+}, resulting in a more pronounced impact on the [SiO_4] and [AlO_4] tetrahedra.

(4) The synthesized NaX-600, 3, 1.2 and NaX-800, 3, 1.2 are effective in reducing exchangeable Cd content in contaminated soil from 3.51 to 2.79 and 1.36 mg/kg, respectively. Further optimization of the Si/Al ratio and pore structure of NaX zeolite could enhance its remediation performance for both Cd and Pb in water and soil.

■ ASSOCIATED CONTENT

Supporting Information

The Supporting Information is available free of charge at https://pubs.acs.org/doi/10.1021/acsomega.4c07708.

Determination of Cd^{2+} and Pb^{2+} concentrations using a UV−visible spectrophotometer; description of adsorption kinetics experiments, adsorption isotherm experi-

https://doi.org/10.1021/acsomega.4c07708
ACS Omega 2024, 9, 51237−51252

ments, effects of adsorbent dosage and initial pH, and material characterization; the effect of adsorption time on the adsorption performance of NaX-800, 3, 1.2 sample (Figure S1); kinetic fitting curves of the NaX-800, 3, 1.2 sample (Figure S2); the effect of initial concentration on the adsorption capacity for Cd^{2+} and Pb^{2+} (Figure S3); isotherm fitting curves of the NaX-800, 3, 1.2 sample (Figure S4); the effect of adsorbent dosage on the adsorption of Cd^{2+} and Pb^{2+} (Figure S5); the effect of pH value on the adsorption of Cd^{2+} and Pb^{2+} (Figure S6); energy dispersive spectra of NaX-600, 3, 1.2 (Cd), and NaX-600, 3, 1.2 (Pb) (Figure S7); energy dispersive spectra of NaX-800, 3, 1.2 (Cd) and NaX-800, 3, 1.2 (Pb) (Figure S8); the N_2 adsorption−desorption isotherms of NaX samples (Figure S9) (PDF)

AUTHOR INFORMATION

Corresponding Author

Lu Bai − *State Key Laboratory of Water Resource Protection and Utilization in Coal Mining, Beijing 102211, China; National Institute of Clean-and-Low-Carbon Energy (NICE), Beijing 102211, China*; Email: lu.bai.a@chnenergy.com.cn

Authors

Zhibing Chang − *School of Chemical and Environmental Engineering, China University of Mining and Technology, Beijing 100083, China;* orcid.org/0000-0002-3339-0020

Yinuo Yan − *School of Chemical and Environmental Engineering, China University of Mining and Technology, Beijing 100083, China*

Nan Guo − *State Key Laboratory of Water Resource Protection and Utilization in Coal Mining, Beijing 102211, China; National Institute of Clean-and-Low-Carbon Energy (NICE), Beijing 102211, China*

Zhenguo Xing − *State Key Laboratory of Water Resource Protection and Utilization in Coal Mining, Beijing 102211, China; National Institute of Clean-and-Low-Carbon Energy (NICE), Beijing 102211, China*

Chunwei Lu − *School of Chemical and Environmental Engineering, China University of Mining and Technology, Beijing 100083, China*

Complete contact information is available at: https://pubs.acs.org/10.1021/acsomega.4c07708

Notes

The authors declare no competing financial interest.

ACKNOWLEDGMENTS

This work was supported by the CHN Energy Investment Group (GJNY-22-92), the Open Fund of State Key Laboratory of Water Resource Protection and Utilization in Coal Mining (GJNY-21-41-19), the Fundamental Research Funds for the Central Universities (2023ZKPYHH02) and the China Scholarship Council (202306430017).

REFERENCES

(1) Chen, N. C.; Zheng, Y. J.; He, X. F.; Li, X. F.; Zhang, X. X. Analysis of the report on the national general survey of soil contamination. *J. Agro-Environ. Sci.* **2017**, *36*, 1689−1692.

(2) Zhou, X.; Wang, Y. P.; Song, Z. Heavy metal contamination and ecological risk assessments in urban mangrove sediments in Zhanjiang bay, South China. *ACS Omega* **2022**, *7*, 21306−21316.

(3) Serrano, M. F.; López, J. E.; Henao, N.; Saldarriaga, J. F. Phosphorus-loaded biochar-assisted phytoremediation to immobilize cadmium, chromium, and lead in soils. *ACS Omega* **2024**, *9* (3), 3574−3587, DOI: 10.1021/acsomega.3c07433.

(4) Wang, X.; Qi, F.; Xiong, J.; Zhao, J.; Zhang, G.; Afzal, S.; Gu, X.; Li, Q.; Luo, S.; Mo, H. Synthesis of a novel dithiocarbamate surfactant derivative adsorbent for efficient removal of heavy metal ions. *ACS Omega* **2023**, *8*, 41512−41522.

(5) Fato, T. P.; Li, D. W.; Zhao, L. J.; Qiu, K.; Long, Y. T. Simultaneous removal of multiple heavy metal ions from river water using ultrafine mesoporous magnetite nanoparticles. *ACS Omega* **2019**, *4*, 7543−7549.

(6) Zhang, X.; Li, C.; Zheng, S.; Di, Y.; Sun, Z. A review of the synthesis and application of zeolites from coal-based solid wastes. *Int. J. Miner. Metall. Mater.* **2022**, *29* (1), 1−21.

(7) Lu, X.; Shi, D.; Chen, J. Sorption of Cu^{2+} and Co^{2+} using zeolite synthesized from coal gangue: isotherm and kinetic studies. *Environ. Earth Sci.* **2017**, *76*, 591 DOI: 10.1007/s12665-017-6923-z.

(8) Ge, Q.; Moeen, M.; Tian, Q.; Xu, J.; Feng, K. Highly effective removal of Pb^{2+} in aqueous solution by Na-X zeolite derived from coal gangue. *Environ. Sci. Pollut. Res.* **2020**, *27*, 7398−7408.

(9) Bu, N.; Liu, X.; Song, S.; Liu, J.; Yang, Q.; Li, R.; Zheng, F.; Yan, L.; Zhen, Q.; Zhang, J. Synthesis of NaY zeolite from coal gangue and its characterization for lead removal from aqueous solution. *Adv. Powder Technol.* **2020**, *31*, 2699−2710.

(10) Jin, Y.; Li, L.; Liu, Z.; Zhu, S.; Wang, D. Synthesis and characterization of low-cost zeolite NaA from coal gangue by hydrothermal method. *Adv. Powder Technol.* **2021**, *32*, 791−801.

(11) Chen, J.; Lu, X. Synthesis and characterization of zeolites NaA and NaX from coal gangue. *J. Mater. Cycles Waste Manage.* **2018**, *20*, 489−495.

(12) Liang, Z.; Gao, Q.; Wu, Z.; Gao, H. Removal and kinetics of cadmium and copper ion adsorption in aqueous solution by zeolite NaX synthesized from coal gangue. *Environ. Sci. Pollut. Res.* **2022**, *29*, 84651−84660.

(13) Yan, K.; Zhang, J.; Liu, D.; Meng, X.; Guo, Y.; Cheng, F. Feasible synthesis of magnetic zeolite from red mud and coal gangue: Preparation, transformation and application. *Powder Technol.* **2023**, *423*, 118495.

(14) Zhou, J.; Zheng, F.; Li, H.; Wang, J.; Bu, N.; Hu, P.; Gao, J. M.; Zhen, Q.; Bashir, S.; Liu, J. L. Optimization of post-treatment variables to produce hierarchical porous zeolites from coal gangue to enhance adsorption performance. *Chem. Eng. J.* **2020**, *381*, 122698 DOI: 10.1016/j.cej.2019.122698.

(15) Li, H.; Zheng, F.; Wang, J.; Zhou, J.; Huang, X.; Chen, L.; Hu, P.; Gao, J. M.; Zhen, Q.; Bashir, S.; Liu, J. L. Facile preparation of zeolite-activated carbon composite from coal gangue with enhanced adsorption performance. *Chem. Eng. J.* **2020**, *390*, 124513 DOI: 10.1016/j.cej.2020.124513.

(16) Li, H.; Li, M.; Zheng, F.; Wang, J.; Chen, L.; Hu, P.; Zhen, Q.; Bashir, S.; Liu, J. L. Efficient removal of water pollutants by hierarchical porous zeolite-activated carbon prepared from coal gangue and bamboo. *J. Cleaner Prod.* **2021**, *325*, 129322.

(17) Zheng, R.; Feng, X.; Zou, W.; Wang, R.; Yang, D.; Wei, W.; Li, S.; Chen, H. Converting loess into zeolite for heavy metal polluted soil remediation based on "soil for soil-remediation" strategy. *J. Hazard. Mater.* **2021**, *412*, 125199.

(18) Yang, D.; Ge, Q.; Feng, X.; Wang, R.; Li, S.; Wei, W.; Zheng, R.; Zhang, J.; Chen, H. Soil for soil remediation" strategy driven on converting natural soils into Fe_2O_3-CAN-Type zeolite composites for dual ionic heavy metal-contaminated soil remediation: Universality, synergistic effects, and mechanism. *ACS ES&T Eng.* **2023**, *3*, 714−724.

(19) Gondek, K.; Mierzwa-Hersztek, M.; Jarosz, R. Effect of willow biochar and fly ash-derived zeolite in immobilizing heavy metals and

promoting enzymatic activity in a contaminated sandy soil. *Catena* **2023**, *232*, 107429.
(20) Ibrahim, E. A.; El-Sherbini, M. A. A.; Selim, E. M. M. Effects of biochar, zeolite and mycorrhiza inoculation on soil properties, heavy metal availability and cowpea growth in a multi-contaminated soil. *Sci. Rep.* **2023**, *13*, 6621 DOI: 10.1038/s41598-023-33712-z.
(21) Zheng, X. J.; Chen, M.; Wang, J. F.; Liu, Y.; Liao, Y. Q.; Liu, Y. C. Assessment of zeolite, biochar, and their combination for stabilization of multimetal-contaminated soil. *ACS Omega* **2020**, *5*, 27374−27382.
(22) Peng, Z.; Wen, J.; Liu, Y.; Zeng, G.; Yi, Y.; Fang, Y.; Zhang, S.; Deng, J.; Cai, X. Heavy metal leachability in soil amended with zeolite- or biochar-modified contaminated sediment. *Environ. Monit. Assess.* **2018**, *190*, 751 DOI: 10.1007/s10661-018-7124-2.
(23) Li, Z.; Wu, L.; Sun, S.; Gao, J.; Zhang, H.; Zhang, Z.; Wang, Z. Disinfection and removal performance for *Escherichia coli*, toxic heavy metals and arsenic by wood vinegar-modified zeolite. *Ecotoxicol. Environ. Saf.* **2019**, *174*, 129−136.
(24) Ma, Y.; Cheng, L.; Zhang, D.; Zhang, F.; Zhou, S.; Ma, Y.; Guo, J.; Zhang, Y.; Xing, B. Stabilization of Pb, Cd, and Zn in soil by modified-zeolite: Mechanisms and evaluation of effectiveness. *Sci. Total Environ.* **2022**, *814*, 152746.
(25) Ribeiro, P. G.; da, O. O.; Aragão, S.; Martins, G. C.; Rodrigues, M.; Souza, J. M. P.; de Souza Moreira, F. M.; Li, Y. C.; Guilherme, L. R. G. Hydrothermally-altered feldspar reduces metal toxicity and promotes plant growth in highly metal-contaminated soils. *Chemosphere* **2022**, *286*, 131768 DOI: 10.1016/j.chemosphere.2021.131768.
(26) Watanabe, H.; Ohmori, H. Dual-wavelength spectrophotometric determination of cadmium with cadion. *Talanta* **1979**, *26*, 959−961.
(27) Xiong, Y.; Zhu, F.; Zhao, L.; Jiang, H.; Zhang, Z. Heavy metal speciation in various types of fly ash from municipal solid waste incinerator. *J. Mater. Cycles Waste Manage.* **2014**, *16*, 608−615.
(28) Ke, G.; Shen, H.; Yang, P. Synthesis of X-zeolite from waste basalt powder and its influencing factors and synthesis mechanism. *Materials* **2019**, *12*, 3895.
(29) Zhang, X.; Tang, D.; Zhang, M.; Yang, R. Synthesis of NaX zeolite: Influence of crystallization time, temperature and batch molar ratio SiO_2/Al_2O_3 on the particulate properties of zeolite crystals. *Powder Technol.* **2013**, *235*, 322−328.
(30) Qian, T.; Li, J. Synthesis of Na-A zeolite from coal gangue with the in-situ crystallization technique. *Adv. Powder Technol.* **2015**, *26*, 98−104.
(31) Verrecchia, G.; Cafiero, L.; de Caprariis, B.; Dell'Era, A.; Pettiti, I.; Tuffi, R.; Scarsella, M. Study of the parameters of zeolites synthesis from coal fly ash in order to optimize their CO_2 adsorption. *Fuel* **2020**, *276*, 118041 DOI: 10.1016/j.fuel.2020.118041.
(32) Kong, D.; Jiang, R. Preparation of NaA zeolite from high iron and quartz contents coal gangue by acid leaching-alkali melting activation and hydrothermal synthesis. *Crystals* **2021**, *11*, 1198.
(33) Monzón, J.; Pereyra, A. M.; Conconi, M. S.; Basaldella, E. I. Phase transformations during the zeolitization of fly ashes. *J. Environ. Chem. Eng.* **2017**, *5*, 1548−1553.
(34) Yang, L.; Qian, X.; Yuan, P.; Bai, H.; Miki, T.; Men, F.; Li, H.; Nagasaka, T. Green synthesis of zeolite 4A using fly ash fused with synergism of NaOH and Na_2CO_3. *J. Cleaner Prod.* **2019**, *212*, 250−260.
(35) Li, Q.; Lv, L.; Zhao, X.; Wang, Y.; Wang, Y. Cost-effective microwave-assisted hydrothermal rapid synthesis of analcime-activated carbon composite from coal gangue used for Pb^{2+} adsorption. *Environ. Sci. Pollut. Res.* **2022**, *29*, 77788−77799.
(36) Hameed, B. H.; Rahman, A. A. Removal of phenol from aqueous solutions by adsorption onto activated carbon prepared from biomass material. *J. Hazard. Mater.* **2008**, *160*, 576−581.
(37) Tseng, R. L.; Wu, F. C. Inferring the favorable adsorption level and the concurrent multi-stage process with the Freundlich constant. *J. Hazard. Mater.* **2008**, *155*, 277−287.
(38) Nakayama, M.; Yano, J.; Nakaoka, K.; Ogura, K. Spectroscopic studies on the incorporation of polypyrrole into zeolite channels. *Synth. Met.* **2003**, *138*, 419−422.
(39) Lyu, F.; Niu, S. L.; Wang, L.; Liu, R. Q.; Sun, W.; He, D. D. Efficient removal of Pb(II) ions from aqueous solution by modified red mud. *J. Hazard. Mater.* **2021**, *406*, No. 124678.
(40) Król, M.; Mozgawa, W.; Jastrzbski, W.; Barczyk, K. Application of IR spectra in the studies of zeolites from D4R and D6R structural groups. *Microporous Mesoporous Mater.* **2012**, *156*, 181−188.
(41) Velarde, L.; Nikjoo, D.; Escalera, E.; Akhtar, F. Bolivian natural zeolite as a low-cost adsorbent for the adsorption of cadmium: Isotherms and kinetics. *Heliyon* **2024**, *10*, No. e24006.
(42) Fotovat, F.; Kazemian, H.; Kazemeini, M. Synthesis of Na-A and faujasitic zeolites from high silicon fly ash. *Mater. Res. Bull.* **2009**, *44*, 913−917.
(43) Yang, T.; Han, C.; Liu, H.; Yang, L.; Liu, D.; Tang, J.; Luo, Y. Synthesis of Na-X zeolite from low aluminum coal fly ash: Characterization and high efficient As(V) removal. *Adv. Powder Technol.* **2019**, *30*, 199−206.

https://doi.org/10.1021/acsomega.4c07708
ACS Omega 2024, 9, 51237−51252